JOURNAL OF QUATERNARY SCIENCE (2019) 1–12 ISSN 0267-8179. DOI: 10.1002/jqs.3146

JQS Journal of Quaternary Science QRA Quaternary Research Association

# Evolution of sea-surface conditions on the northwestern Greenland margin during the Holocene

MYRIAM CARON,[1]* ANDRÉ ROCHON,[1] JEAN-CARLOS MONTERO-SERRANO[1] and GUILLAUME ST-ONGE[1,2]
[1]Institut des sciences de la mer de Rimouski (ISMER), Université du Québec à Rimouski and GEOTOP Research Center, Canada
[2]Canada Research Chair in Marine Geology

Received 29 November 2018; Revised 31 July 2019; Accepted 23 August 2019

ABSTRACT: Reconstructions of sea-surface conditions during the Holocene were achieved on two sediment cores from the northwest Greenland margin (AMD14-204) and Kane Basin (AMD14-Kane2B) based on dinoflagellate cyst assemblages. On the northwest Greenland margin, sea-surface conditions were cold with an extended sea ice cover prior to 7750 cal a BP associated with the end of the deglaciation. A major change occurred around ca. 7750 cal a BP with enhanced influence of warmer water from the West Greenland Current, and optimal sea-surface conditions were observed around 6000 cal a BP. After 3350 cal a BP, results reflect the establishment of the modern assemblages. In the Kane Basin, sea-surface conditions were not favourable for dinocyst productivity prior to 7880 cal a BP, as the basin was still largely covered by ice. The presence of warmer water is recorded between 7880 and 7200 cal a BP and the highest primary productivity between 5200 and 2100 cal a BP, but sea-surface conditions remained cold with an extended sea ice cover throughout the Holocene. Overall, the results from this study revealed the strong influence of meltwater discharges and oceanic current variability on the sea-surface conditions. Copyright © 2019 John Wiley & Sons, Ltd.

KEYWORDS: Baffin Bay; dinoflagellate cysts; Kane Basin; Melville Bay; sea-surface conditions.

## Introduction

Over recent decades, modern climate warming has resulted in a considerable reduction of sea ice extent and cover duration in the Arctic (Serreze and Stroeve, 2015) and to place these rapid changes in a long-term perspective, there is a need for better understanding of the interactions between sea ice and climate throughout the geological past (Jakobsson *et al.*, 2010; Müller and Stein, 2014). Baffin Bay is an excellent location to study these interactions as sea ice is present inside the bay during most of the year (Tang *et al.*, 2004) and because it plays the role of oceanic corridor between the Arctic and the North Atlantic oceans (through the Labrador Sea, where deep convection contributes to the thermohaline circulation). Moreover, Baffin Bay has been affected by the dynamics of three large ice sheets (Greenland (GIS), Innuitian (IIS) and Laurentide ice sheets) since the last glacial maximum (England *et al.*, 2006). Therefore, it is highly relevant to investigate how oceanographic and climatic changes have affected the sea-surface conditions in Baffin Bay since the last deglaciation.

Dinoflagellate cysts (hereafter, dinocysts) are excellent tracers for the estimation of past sea-surface conditions, as their highly resistant organic membrane (e.g., Fensome *et al.*, 1993) allows them to be preserved in the sediment, particularly in subpolar and polar seas where they are found in abundance and high diversity (e.g., Mudie, 1992; Matthiessen, 1995; Mudie *et al.*, 2001). Several oceanographic properties can be reconstructed from dinocyst assemblages including sea-surface temperature (SST), salinity (SSS), seasonal sea ice cover (SIC), and primary productivity (de Vernal *et al.*, 2001, 2013a; Radi and de Vernal, 2008). Previous studies based on dinocysts, but also diatoms, molluscs, foraminifera and sea ice biomarkers ($IP_{25}$) have contributed to our knowledge of past sea-surface conditions in Baffin Bay (e.g., Knudsen *et al.*, 2008; Krawczyk *et al.*, 2017). However, information available on the northeastern Baffin Bay (Melville Bay) and Nares Strait sea-surface variability during the Holocene is still incomplete, as studies have mainly focused on the regions of the North Water Polynya (e.g., Levac *et al.*, 2001) and Disko Bay region (e.g., Ribeiro *et al.*, 2012; Allan *et al.*, 2018). In this study, well-preserved dinocyst assemblages of two sediment cores recovered from the Upernavik cross-shelf trough (AMD14-204) and in the Kane Basin (AMD14-Kane2B) were analyzed and data were processed with the modern analogue technique (MAT) to reconstruct sea-surface conditions during the Holocene.

## Environmental setting

Baffin Bay is an oceanic basin 1300 km long and 450 km wide, with a depth of up to 2300 m (Aksu and Piper, 1987). It is connected to the Arctic Ocean through the Canadian Arctic Archipelago straits and to the Atlantic Ocean through the Davis Strait. The Nares Strait separates Ellesmere Island from Greenland and extends north of Baffin Bay up to the Arctic Ocean (Fig. 1). Baffin Bay is influenced by the cold Baffin Island Current (BIC, temperature >-1°C, salinity <34) flowing southward along Baffin Island from northernmost Baffin Bay, and by the relatively warm and salty West Greenland Current (WGC; temperature >2°C, salinity >34) flowing northward (Fig. 1; Tang *et al.*, 2004; Zweng and Münchow, 2006). The WGC consists of a mix of the cold and low salinity East Greenland Current (EGC; Arctic water from the Fram Strait) and the warmer and salty Irminger Current (IC; North Atlantic water), both of which merge south of Greenland to form the WGC (Fig. 1; Tang *et al.*, 2004). The WGC flows northward along the west Greenland shelf and turns west in Melville Bay before joining the BIC in Smith Sound. However, it has been shown that a small branch of the WGC reaches Kane Basin and circulates at depths below 250 m (Sadler, 1976).

*Correspondence: M. Caron, as above.
E-mail: myriam.caron03@uqar.ca

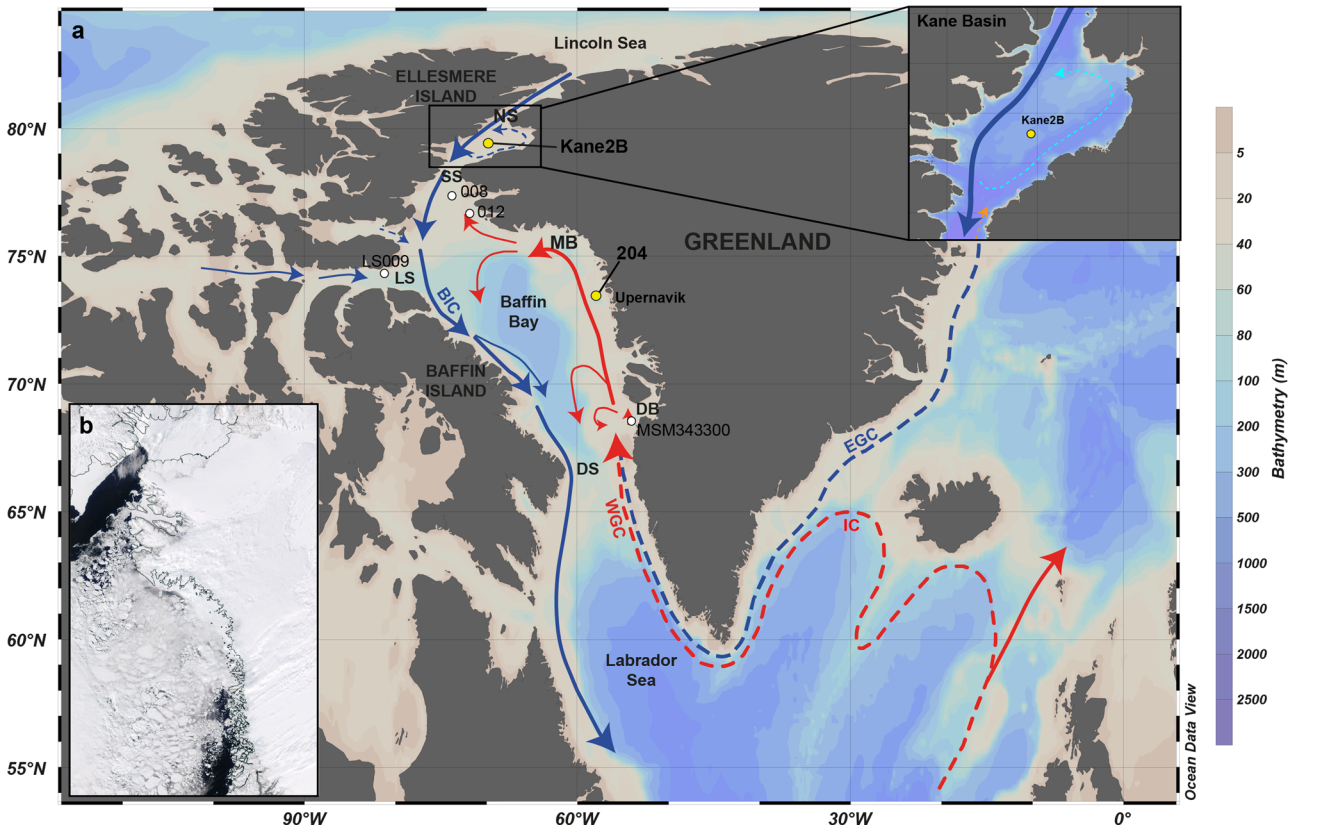


**Figure 1.** (a) Map of Baffin Bay and Nares Strait indicating sampling location for cores AMD14-Kane2B (Kane Basin) and AMD14-204 (Upernavik cross-shelf trough), as well as cores mentioned in this study (MSM343300, sites 008 and 012, LS009). Regional surface oceanic circulation: BIC: Baffin Island Current (Arctic water in blue); WGC: West Greenland Current (in red; mix of IC: Irminger Current, North Atlantic water and EGC: East Greenland Current). NS: Nares Strait; MB: Melville Bay; DB: Disko Bugt; DS: Davis Strait; LS: Lancaster Sound; SS: Smith Sound; NOW: North Water Polynya. (b) Satellite image of the study area indicating the sea ice cover (image from 22 May 2018; credit: NASA Worldview: https://worldview.earthdata.nasa.gov). [Color figure can be viewed at wileyonlinelibrary.com]

Baffin Bay is covered by sea ice during most of the year, with a minimal extent in September (Tang *et al.*, 2004). Nevertheless, the SIC distribution in Baffin Bay is asynchronous with sea ice extending further southward on the east than the west side due to the differences in temperature and salinity of the two major surface currents (WGC and BIC) flowing in opposite directions (Tang *et al.*, 2004). Ice floes and icebergs are present continually in the Nares Strait, even during summer (Münchow *et al.*, 2006). Landfast ice during winter leads to the formation of an ice arch in the Kane Basin, which marks the boundary with the North Water Polynya (Barber *et al.*, 2001; Kwok *et al.*, 2010).

## Material and methods

Two Calypso Square cores were collected on board the CCGS icebreaker Amundsen in northern Baffin Bay during the 2014 ArcticNet expedition: core AMD14-204 (hereinafter referred to as 204) located on the northwest Greenland margin, and core AMD14-Kane2B (hereinafter referred to as Kane2B) located in the Kane Basin (Fig. 1; Table 1). The chronology of core 204 was established using an approach combining radiocarbon dating ($\Delta R = 140\pm30$ years) with paleomagnetic chronostratigraphic markers (Caron *et al.*, 2019) and organic matter dating (Giraudeau *et al.*, under review). The chronology of core Kane2B was established by Georgiadis *et al.* (2018) based on 20 radiocarbon ages from mixed benthic foraminifera and mollusc shell fragments ($\Delta R = 240\pm51$ years). Based on the established chronologies, core 204 covers the last ca. 9100 cal a BP, and has a mean sedimentation rate of 95 cm ka$^{-1}$, while core Kane2B covers the last ca. 9000 cal a BP, and has sedimentation rates ranging from 20 to 220 cm ka$^{-1}$ (Fig. S1).

### *Palynological preparations and analyses*

Palynological analyses were performed at 8 cm intervals with a volume of ~5 cm$^3$ of wet sediment following the protocol described by Rochon *et al.* (1999). Marker grains (*Lycopodium clavatum* spore tablets, batch n°414831, Lund University) were added to each sample to estimate palynomorph concentrations following the method described by Matthews (1969) and Mertens *et al.* (2009). The concentrations (cysts cm$^{-3}$) were multiplied by the sedimentation rate (cm yr$^{-1}$) in each sample in order to describe the abundance as influxes (cysts cm$^{-2}$ yr$^{-1}$). This makes it easier to assess changes in dinoflagellate and benthic (organic linings of foraminifera) productivities in environments where sedimentation rates vary through time. After wet sieving the samples at 100 and 10 µm to eliminate sand, fine silt and clay, the 10–100 µm fraction was chemically treated with hydrochloric acid (HCl, 10%) to eliminate carbonates and

**Table 1.** Coordinates of the two cores used in this study.

| Core ID | Region | Latitude (°N) | Longitude (°W) | Water depth (m) | Core length (cm) |
|---|---|---|---|---|---|
| AMD14-204 | Upernavik Isstrøm | 73°15.663′ | 57°53.987′ | 987 | 734 |
| AMD14-Kane2B | Kane Basin | 79°30.908′ | 70°49.742′ | 220 | 425 |

hydrofluoric acids (HF, 49%) to eliminate silicates. The residual organic matter was mounted on microscope slides with glycerin gelatin, and slides were analyzed using a transmitted light microscope at magnifications of 400x to 1000x. Dinocysts and organic linings of foraminifera were identified and counted (Fig. 2) until reaching a minimum of 300 dinocysts and 100 marker grains in each sample. Reworked and freshwater palynomorphs were also counted. Organic linings of foraminifera observed in the samples are mainly benthic, as they are more resistant to dissolution than those of planktic foraminifera (de Vernal *et al.*, 1992). The identification of dinocysts followed the nomenclature provided by Rochon *et al.* (1999), Head *et al.* (2001), Radi *et al.* (2013), Mertens *et al.* (2018) and Londeix *et al.* (2018).

## *Statistical approach and data analyses*

The MAT allowed the reconstruction of sea-surface conditions using a dinocyst database for the Northern Hemisphere that includes 1776 reference sites and 73 taxa (Allan *et al.*, 2018). The calculations were performed using the Bioindic scripts developed for the R platform by Joel Guiot (CEREGE, France) and the procedure described by de Vernal *et al.* (2013b). The MAT relies on the hypothesis that similar biogenic assemblages occur under similar environmental conditions without any assumptions in terms of quantitative relationships (Guiot and de Vernal, 2007). Although there have been some concerns expressed that root mean square error of prediction might be underestimated (Telford, 2006; Telford and Birks, 2005, 2011), this method (MAT) has been demonstrated to be

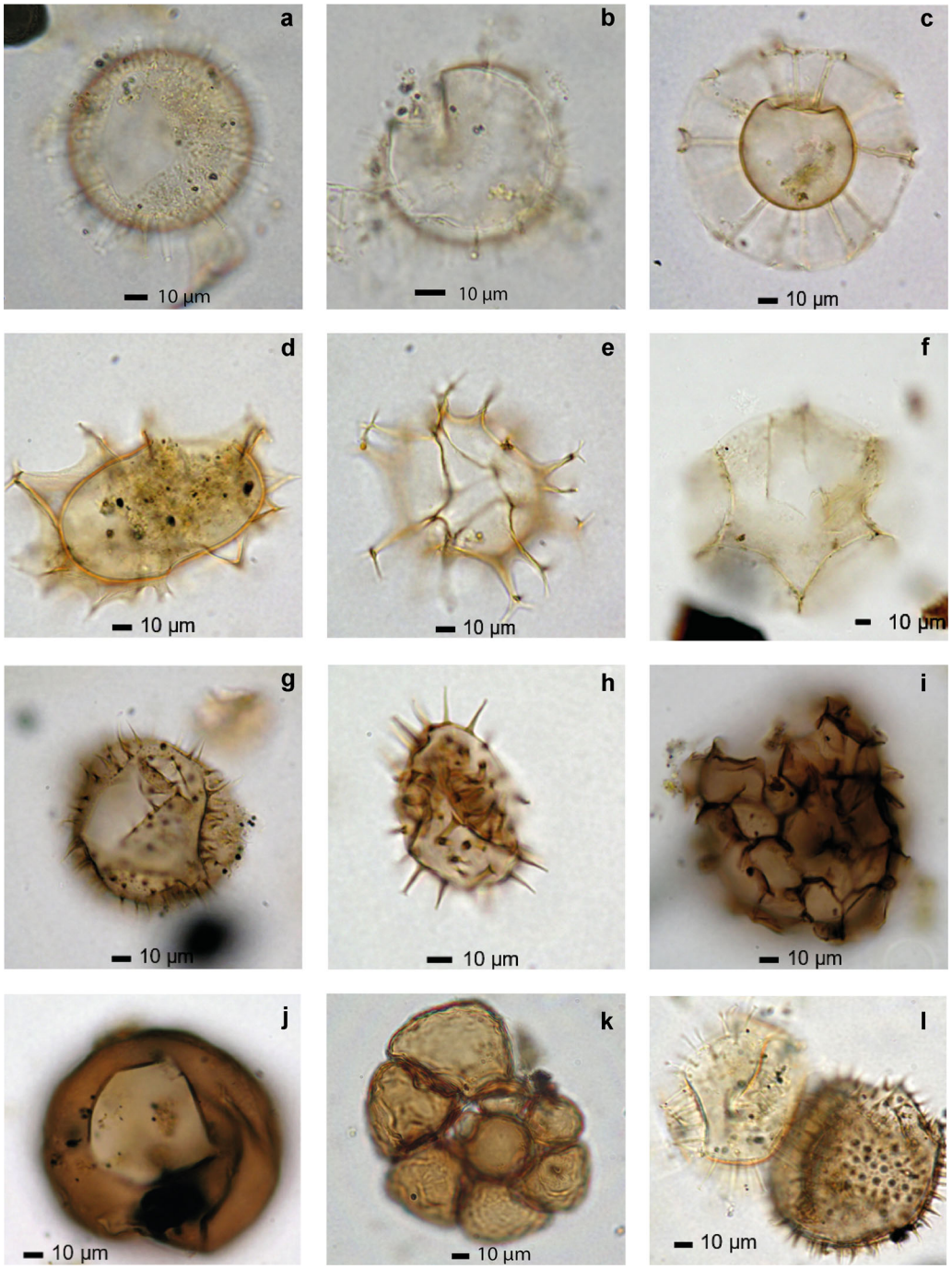


**Figure 2.** Photoplate of main dinocyst taxa and palynomorphs (foraminiferal lining) identified in this study: (a) *Operculodinium centrocarpum* sensu Wall and Dale; (b) Cyst of *Pentapharsodinium dalei*; (c) *Nematosphaeropsis labyrinthus*; (d) *Spiniferites elongatus*; (e) *Spiniferites ramosus*; (f) *Impagidinium pallidum*; (g) *Islandinium minutum*; (h) *Echinidinium karaense*; (i) *Polykrikos* var. Arctic; (j) *Brigantedinium* simplex; (k) foraminiferal lining; (l) *O. centrocarpum* (left) + *I. minutum* (right). [Color figure can be viewed at wileyonlinelibrary.com]

as reliable as any reconstruction method using micropaleontological proxies (Guiot and de Vernal, 2011).

Five analogues were used, and a logarithmic transformation was applied on the relative abundance of dinocysts for the reconstructions. The errors of prediction on winter and summer SSTs are ±1.4/1.7°C, and ±1.2/2.1 for SSSs. The SIC extent is expressed in number of months with more than 50% ice coverage (based on the 1953–2003 mean) (±1.4 months/year) and productivity in gC $m^{-2}$ $yr^{-1}$ (±61.5 gC $m^{-2}$ $yr^{-1}$). The heterotrophic/autotrophic (H/A) dinocyst ratio was calculated to assess temporal changes in the dominant trophic mode. Finally, principal component analyses were performed with the software PAST (Hammer *et al.*, 2001) to differentiate the distribution of assemblages (taxa <1% were excluded).

## Results

The two cores used in this study (204 and Kane2B) were described in detail by Caron *et al.* (2019) and Georgiadis *et al.* (2018) and major sedimentological units (Fig. S1) were distinguished based on the lithology and physical properties of the sediment. Overall, the lithology of core 204 is relatively homogeneous and fine grained and is largely dominated by hemipelagic sedimentation. By contrast, core Kane2B shows a more variable sedimentation associated with higher inputs of ice-rafted debris and reworked sediments throughout the core (Caron *et al.*, 2019; Georgiadis *et al.*, 2018). Palynological results provide additional details on environmental changes for both cores. A total of 25 dinocyst taxa were identified, 14 of which account for more than 95% of the assemblages (Table 2 and Fig. 2). One interval at the base of core Kane2B (428–300 cm, ca. 9000–8300 cal a BP) was not considered for palynological reconstructions due to very low dinocyst concentrations. Relative abundance of the main taxa accounting for more than 95% of the assemblages is presented in Figs. 3 and 5. Main dinocyst assemblage zones were distinguished based on the scores of the first two components of the principal component analyses (Fig. S2), reflecting the occurrence of accompanying taxa and changes in abundance of the dominant species. Reconstructions of sea-surface properties including SST, SSS, SIC and primary productivity are shown in Figs. 4 and 6, together with organic linings of foraminifera, freshwater (*Halodinium*) and reworked palynomorph influxes. The reconstructed primary productivity represents the productivity of all autotrophic groups (including diatoms, ciliates, etc.; e.g., Cormier *et al.*, 2016).

### *AMD14-204 – Northwestern Greenland margin*

Dinocyst assemblages were recovered from all samples in core 204, with an average estimated flux of 1260 ± 100 cysts $cm^{-2}$ $yr^{-1}$, and a maximum value of 4830 cysts $cm^{-2}$ $yr^{-1}$ between ca. 5700 and 5600 cal a BP (Fig. 3). Overall, reconstructed SST ranged from -1.7 to 7°C, summer SSS ranged from 27 to 32.8, SIC between 3 and 9 months per year and primary productivity between 90 and 190 gC $m^{-2}$ $yr^{-1}$ (Fig. 4). The characteristics of each dinocyst assemblage zone are described below in terms of relative abundance and sea-surface condition reconstructions:

**Zone 1** (prior to 7750 cal a BP; 738–604 cm) is characterized by the dominance of heterotrophic taxa, such as *Islandinium minutum* (up to 39%) and *Brigantedinium* spp. (up to 46%), as revealed by the H/A ratio (Fig. 4). It is also characterized by the highest relative abundance of *Impagidinium pallidum* (up to 4%), and *Polykrikos* var. Arctic (up to 3.5%), which nearly disappears after 7750 cal a BP (Fig. 3). Sea-surface reconstructions reveal the lowest SST values (summer SST averaging ~2°C) and the maximum SIC duration (8–9 months/year) of the entire core (Fig. 4).

**Zone 2** (7750–3350 cal a BP; 604–164 cm) is dominated by "warmer water" autotrophic species (Rochon *et al.*, 1999; Zonneveld *et al.*, 2013), including *Operculodinium centrocarpum* and *Spiniferites elongatus,* and by the gradual increase of the cyst of *Pentapharsodinium dalei* (from ~7 to 37%). The dominance of these autotrophic species after 7750 cal a BP is reflected by the low H/A ratio (Fig. 4). Assemblage zone 2 was subdivided into five subzones, which coincide with the maximum (subzones 2a, 2c and 2e) and minimum (subzones 2b and 2d) relative abundance of *O. centrocarpum* (Figs. 3 and S2). Subzone 2a (7750–6880 cal a BP; 604–521 cm) is characterized by the sharp increase of *O. centrocarpum*, *S. elongatus* and *S. ramosus*, the decrease of *I. minutum* and *Brigantedinium* spp. and near disappearance of *Polykrikos* var. Arctic. The transition between subzones 2a and 2b (6880–6450 cal a BP; 521–475 cm) is marked by the arrival of *Nematosphaeropsis labyrinthus*, the low abundance of *O. centrocarpum* and the increase of heterotrophic taxa (*Echinidinium karaense*, *I. minutum* and *Brigantedinium* spp.; Fig. 3). Subzone 2c (6450–5100 cal a BP; 475–300 cm) corresponds to the highest abundance of *O. centrocarpum* (up to 67%), *S. elongatus* (up to 18%) and *S. ramosus*, and low abundance of all heterotrophic taxa (Fig. 3). It is also characterized by the highest production of organic linings of foraminifera (up to 1500 linings $cm^{-2}$ $yr^{-1}$; Fig. 4). Subzone 2d (5100–4750 cal a BP; 300–282 cm) is characterized by the maximum abundance of *E. karaense* and sharp decrease of the gonyaulacacean taxa (*O. centrocarpum*, *S. ramosus*, *S. elongatus* and *N. labyrinthus*; Fig. 3). Finally, subzone 2e (4750–3350 cal a BP; 282–164 cm) is characterized by another increase in the abundance of Gonyaulacacean taxa. Overall,

**Table 2.** List of the dominant dinoflagellate cyst taxa from the two cores locations, shown in Fig. 2.

| Dinoflagellate taxa | Trophic mode | | Grouped as |
|---|---|---|---|
| *Operculodinium centrocarpum* sensu Wall and Dale | G | A | *Operculodinium centrocarpum* |
| *O. centrocarpum* short processes | G | A | *Operculodinium centrocarpum* |
| *O. centrocarpum* Arctic | G | A | *Operculodinium centrocarpum* |
| *Nematosphaeropsis labyrinthus* | G | A | |
| *Spiniferites elongatus* | G | A | |
| *Spiniferites ramosus* | G | A | |
| Cyst of *Pentapharsodinium dalei* | P | A | |
| *Impagidinium pallidum* | G | A | |
| *Islandinium minutum* | P | H | |
| *Islandinium brevispinosum* | P | H | *Islandinium minutum* |
| *Islandinium? cezare* | P | H | *Islandinium minutum* |
| *Echinidinium karaense* | P | H | |
| *Brigantedinium* spp. | P | H | |
| *Brigantedinium simplex* | P | H | *Brigantedinium* spp. |
| *Brigantedinium cariacoense* | P | H | *Brigantedinium* spp. |
| *Polykrikos* var. Arctic | P | H | |
| *Polykrikos quadratus* | P | H | *Polykrikos* var. Arctic |

G=Gonyaulacales, P=Peridiniales, A=Autotrophic and H=Heterotrophic taxa.

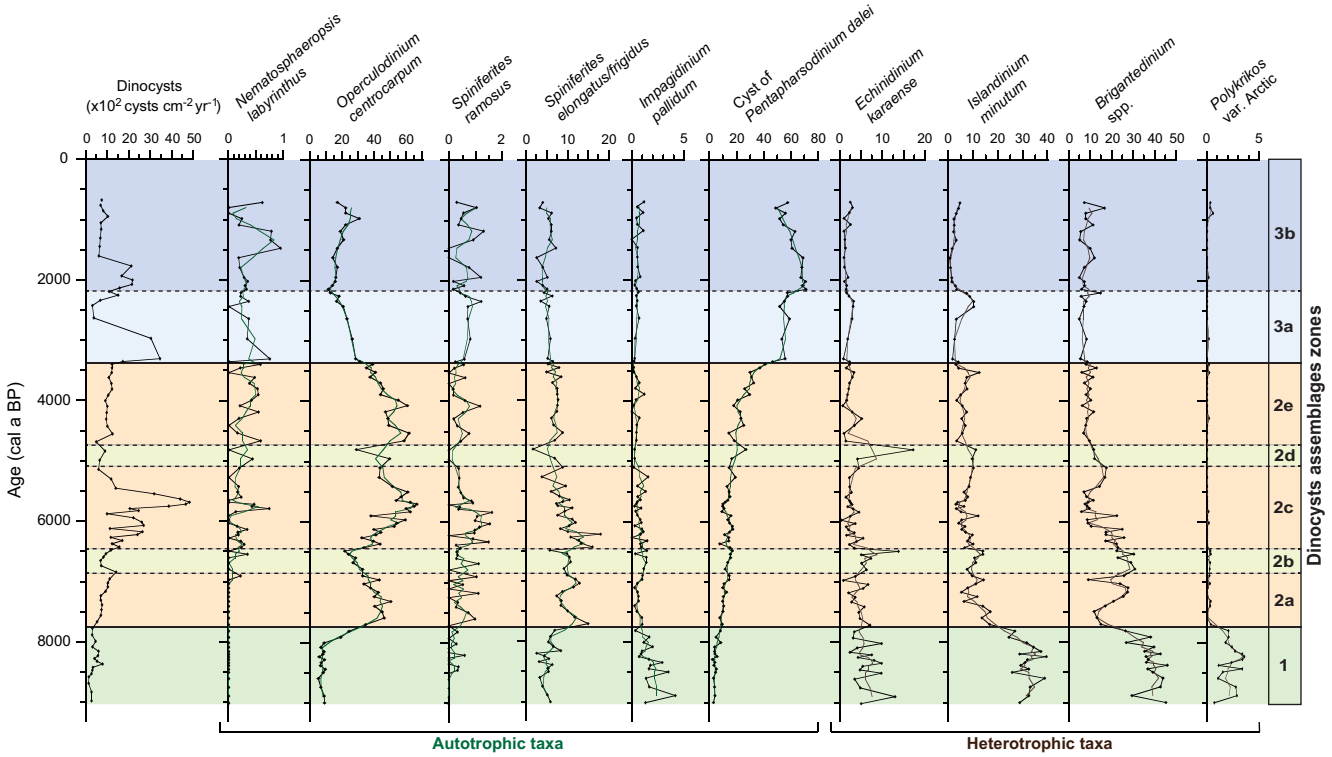


**Figure 3.** Dinocyst influx (x10$^2$ cysts cm$^{-2}$ yr$^{-1}$), relative abundance (%) of the main dinocyst taxa, and dinocyst assemblage zones in core AMD14-204. Data are represented with the thin dotted dark grey lines, 3-points running mean are represented by green (autotrophs) or brown (heterotrophs) lines. [Color figure can be viewed at wileyonlinelibrary.com]

reconstructed SST, SSS and primary productivity conditions display a series of three pulses of high SST values (subzones 2a, 2c and 2e), alternating with two short periods of low values (subzones 2b and 2d) (Fig. 4). The three "warm" pulses are marked by relatively low SIC duration, while the cooler periods are marked by increased SIC, up to 9 months/yr (Fig. 4).

**Zone 3** (3350–700 cal a BP; 164–0 cm) is characterized by the maximum abundance of both the cyst of *P. dalei* (up to 71%; Fig. 3) and *N. labyrinthus*. It is subdivided into two subzones. Subzone 3a (3350–2170 cal a BP; 164–106 cm) is dominated by the cyst of *P. dalei* (avg. ~55%), a decrease of *O. centrocarpum* abundance, relatively stable values of the other "North Atlantic" taxa

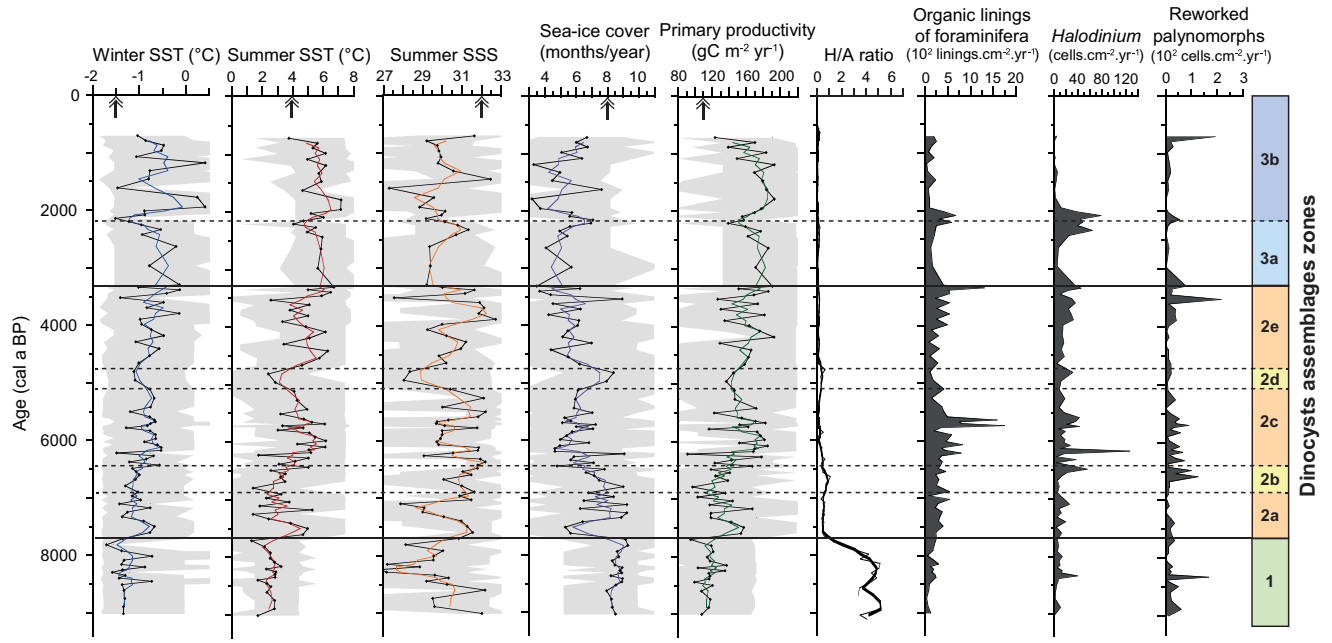


**Figure 4.** Reconstructions of winter and summer salinity (SSS) and sea-surface temperature (SST), seasonal sea ice cover in months/year, and productivity (in gC m$^{-2}$ yr$^{-1}$) based on the modern analogue technique (MAT) applied to dinocyst assemblages in core AMD14-204. Reconstructions are shown with the black lines, the 3-points running mean are represented by bold coloured lines and the maximum and minimum possible values according to the set of five analogues are shown in light grey. Modern values are indicated by a black arrow at the top. Heterotrophs/autotrophs (H/A) ratio and influxes of organic linings of foraminifera, *Halodinium* spp. and reworked palynomorphs are displayed on the right. Statistical minimum and maximum distances between fossil and modern analogues are 0.12 and 0.20, respectively. [Color figure can be viewed at wileyonlinelibrary.com]

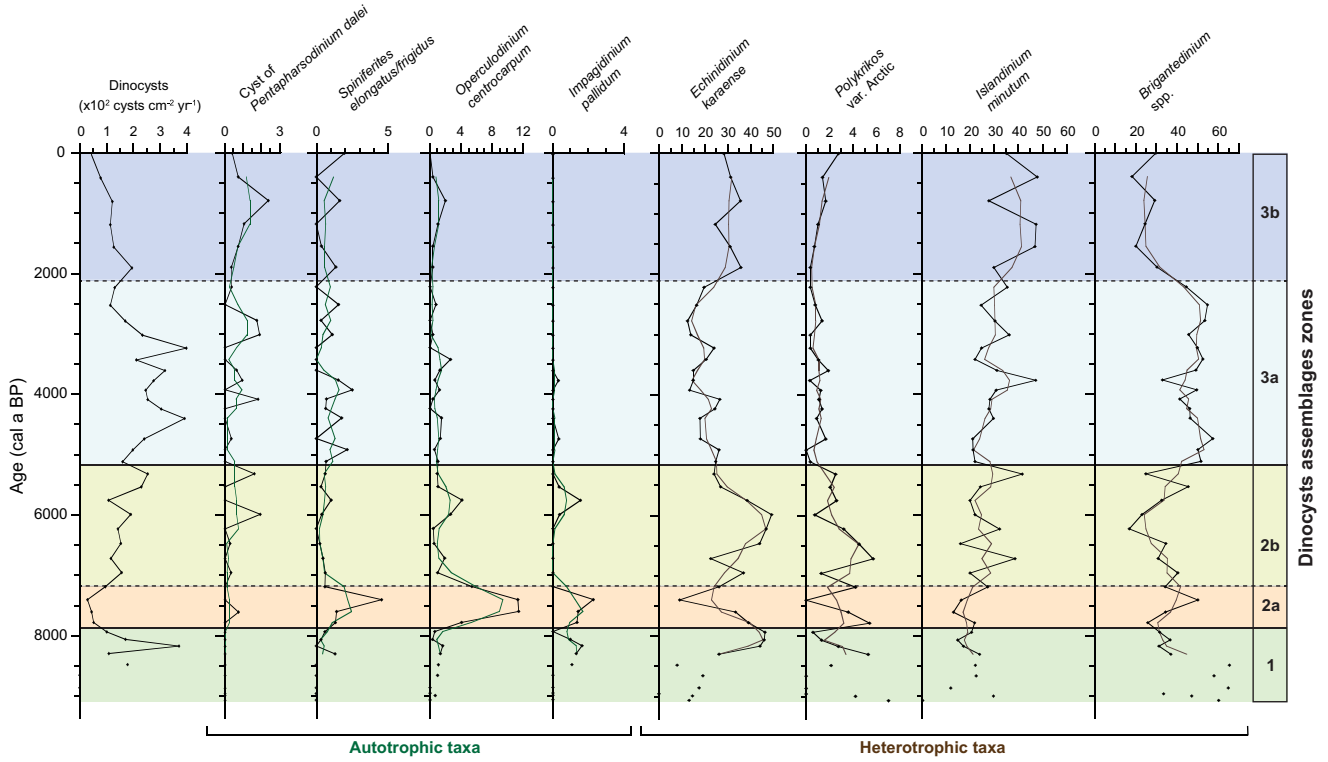


**Figure 5.** Dinocyst influx (x10$^2$ cysts cm$^{-2}$ yr$^{-1}$), relative abundance (%) of the main dinocyst taxa, and dinocyst assemblage zones in core AMD14-Kane2B. Data are represented by the thin dotted dark grey lines, 3-points running mean are represented by green (autotrophs) or brown (heterotrophs) lines. In samples containing sparse assemblages (counts <50 cysts), occurrences are shown by dots on the diagram. [Color figure can be viewed at wileyonlinelibrary.com]

(*S. elongatus*, *N. labyrinthus* and *S. ramosus*), and slightly increasing abundance of *I. minutum* and *E. karaense*. Subzone 3b (2170–700 cal a BP; 106–0 cm) is characterized by the maximal abundance of cysts of *P. dalei,* an increase of *O. centrocarpum* and a peak in the abundance of *N. labyrinthus*. All heterotrophic taxa are at their lowest abundance in this subzone. Sea-surface reconstructions for zone 3 indicate the highest SST and primary productivity values throughout the core, as well as the lowest values of SIC (Fig. 4).

## *AMD14-Kane2B – Kane Basin*

Dinocysts are less abundant in core Kane2B than in core 204 and influxes range from extremely low (barren in dinocysts at the base) to 397 cysts cm$^{-2}$ yr$^{-1}$, with maximum values recorded between

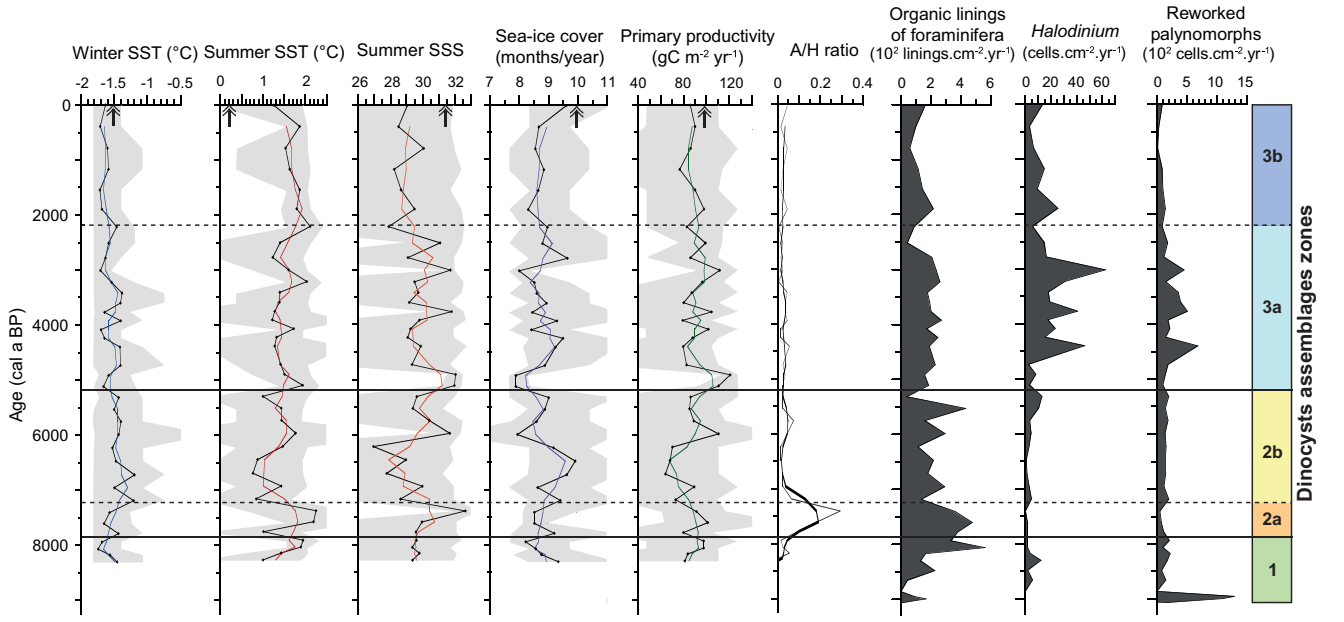


**Figure 6.** Reconstructions of winter and summer salinity (SSS) and sea-surface temperature (SST), seasonal sea ice cover in months/year, and productivity (in gC m$^{-2}$ yr$^{-1}$) based on modern analogue technique (MAT) applied to dinocyst assemblages in core AMD14-Kane2B. Reconstructions are shown with the black lines, the 3-points running means are represented by coloured lines and the maximum and minimum possible values according to the set of five analogues are shown in light grey. Modern values are indicated by a black arrow at the top. Autotrophs/heterotrophs (A/H) ratio and influxes of organic linings of foraminifera, *Halodinium* spp. and reworked palynomorphs are displayed on the right. Statistical minimum and maximum distances between fossil and modern analogues are 0.08 and 0.11, respectively. [Color figure can be viewed at wileyonlinelibrary.com]

4500 and 3000 cal a BP (Fig. 5). Maximum influxes of foraminiferal linings (up to 500 linings $cm^{-2}$ $yr^{-1}$) are recorded between 8100 and 7400 cal a BP (Fig. 6), suggesting higher benthic productivity. Reworked palynomorphs are abundant throughout the core (up to 1200 cells $cm^{-2}$ $yr^{-1}$ at the base of the core; Fig. 6), which suggests high erosion and remobilization of pre-Quaternary sediments. The core is largely dominated by heterotrophic taxa (77–100%) as reflected by the A/H ratio <1 (Fig. 6). Overall, reconstructed SST ranged from -1.8 to 2.2°C, summer SSS ranged from 27 to 33, SIC between 8 and 10 months per year, and primary productivity between 55 and 120 gC $m^{-2}$ $yr^{-1}$.

**Zone 1**: Prior to 8300 cal a BP (427–298 cm), dinocyst abundance was too low to achieve reconstructions. Nonetheless, the few specimens found were mostly of *Brigantedinium* spp., *E. karaense* and *I. minutum*, suggesting harsh sea-surface conditions, likely associated with a perennial or quasi-perennial SIC. A peak of dinocyst influx at 8100 cal a BP is associated with an increase of *E. karaense* (up to 45%) and a slight decrease of *Brigantedinium* spp. (Fig. 5).

**Zone 2** (7880–5200 cal a BP; 270–172 cm) is marked by maximum abundance of autotrophic species (*O. centrocarpum* and *S. elongatus*), although the assemblage remains dominated by heterotrophic taxa, such as *Brigantedinium* spp., *E. karaense* and *I. minutum* (Fig. 5 and A/H ratio, Fig. 6). It is subdivided into two subzones based on the relative abundance of taxa. Subzone 2a (7880–7225 cal a BP; 270–242 cm) is marked by low dinocyst influxes (~60 cysts $cm^{-2}$ $yr^{-1}$) and the appearance of the cyst of *P. dalei*. It is dominated by *Brigantedinium* spp. and accompanied by *I. minutum*, but it also corresponds to the maximal abundance of *O. centrocarpum* (up to 11%), *S. elongatus* (up to 4%) and *I. pallidum* (up to 2%). Sea-surface reconstructions indicate maximum values of summer SST and SSS during this period. Subzone 2b (7225–5200 cal a BP; 242–172 cm) is dominated by *E. karaense* (up to 49%) and *I. minutum* (up to 41%). It is also characterized by the highest relative abundance of *Polykrikos* var. Arctic (up to 5%), an Arctic species restricted to regions characterized by cold surface waters (Zonneveld *et al.*, 2013). Sea-surface reconstruction revealed relatively low summer SST (~1°C), SSS (~27psu) and primary productivity (~60 gC $m^{-2}$ $yr^{-1}$), and an extended SIC during this period (Fig. 6).

**Zone 3** (5200 cal a BP to present; 172–0 cm) is characterized by *Brigantedinium* spp. and a progressive increase of the relative abundance of *I. minutum* (20 to 47%). A change occurred around ca. 2100 cal a BP, which leads to the subdivision into two subzones. Subzone 3a (5200–2100 cal a BP; 172–45 cm) is characterized by the maximum relative abundance of *Brigantedinium* spp. (up to 57%), low abundance of *E. karaense* (~15%), and maximum dinocyst influxes (4500 to 3000 cal a BP). Subzone 3b (2100 cal a BP to present; 45–0 cm) is characterized by the maximum abundance of *I. minutum* (up to 48%) and by increasing abundance of *E. karaense, Polykrikos* var. Arctic and cysts of *P. dalei* (Fig. 5). Sea-surface reconstructions reveal a slight increase in SIC and a slight decrease in SST and primary productivity during this period (Subzone 3b, Fig. 6).

# Discussion

Dinocyst assemblages from two sites (204 and Kane2B) reflect important oceanographic changes throughout the Holocene. The results indicate a shift from cold and extended SIC to milder postglacial conditions with seasonal SIC that occurred around 7880 cal a BP in the Kane Basin and around 7750 cal a BP in the northeast Baffin Bay. The synthesis on the timing of climatic and environmental changes documented from both cores is presented in Figs. 7 and 8. Results from core 204 (Fig. 7) are compared with the regional record from Disko Bugt (MSM343300: Ouellet-Bernier *et al.*, 2014), while results from core Kane2B (Fig. 8) are compared with regional records from Smith Sound (Sites 008 and 012: Levac *et al.*, 2001) and Lancaster Sound (2004-804-009: Ledu *et al.*, 2008).

## *Early Holocene – end of deglaciation*

In both cores, assemblages from this period (prior to 7750 and 7880 cal a BP, respectively) are dominated by *Brigantedinium* spp., *I. minutum*, *E. karaense* and accompanied by *Polykrikos* var. Arctic. The codominance of those taxa is often associated with harsh, densely ice-covered conditions and relatively high productivity (de Vernal *et al.*, 2001, 2013a; Head *et al.*, 2001; Rochon *et al.*, 1999; Zonneveld *et al.*, 2013). Low dinocyst influxes and the dominance of these heterotrophic species suggest primary productivity probably dominated by diatoms, which constitute the main food source of heterotrophic dinoflagellates (e.g., Jacobson and Anderson, 1986). Diatoms are usually advantaged (opportunists) compared with dinoflagellates in areas where nutrients are relatively abundant (e.g., Dale, 1996; Lovejoy *et al.*, 2002).

At the site of core 204, the sea-surface reconstructions revealed the lowest SST values (~2°C in summer, ~-1.4°C in winter) and the highest SIC duration (up to 9 months/year) during this period, although associated with minimal values of productivity (Fig. 4). Harsh sea-surface conditions likely prevented the development of phototrophic dinocyst taxa in this area, while primary producers such as diatoms may account for the presence of heterotrophic dinocyst taxa. Previous studies (e.g., Ouellet-Bernier *et al.*, 2014; Gibb *et al.*, 2015) in the region of Disko Bugt have also observed dinocyst assemblages dominated by heterotrophic taxa prior to 7300 and 7400 cal a BP, respectively. Besides, Jennings *et al.* (2014) determined a continuous GIS mass loss until 7800 cal a BP based on foraminifera and other proxies. Thus, the relatively low reconstructed salinity values in core 204 support evidence of high meltwater discharge from the GIS prior to 7750 cal a BP, also suggested by Caron *et al.* (2019).

In the Kane Basin, immediately after the retreat of grounded ice from the core site, the high concentration of reworked palynomorphs (Fig. 6) associated with a high ice-rafted debris content support ice-proximal conditions with high meltwater discharge from both IIS and GIS (Caron *et al.*, 2019; Georgiadis *et al.*, 2018). This strong meltwater input, linked to the retreating ice sheets, probably resulted in very harsh sea-surface conditions with a quasi-permanent SIC during this period (prior to 8300 cal a BP; Ledu *et al.*, 2010), which would explain the very low concentration of dinocysts observed during this period. Moreover, we consider that this period before 8300 cal a BP is linked to a major oceanographic reorganization associated with the opening of the Nares Strait and establishment of the modern oceanic circulation (e.g., Jennings *et al.*, 2011, 2019; Georgiadis *et al.*, 2018).

## *Onset of full interglacial conditions*

On the northwestern Greenland margin (core 204), a major shift is recorded at around 7750 cal a BP, representing a change in dominant species from heterotrophic to phototrophic taxa. It was also associated with a rapid increase of dinocyst influxes

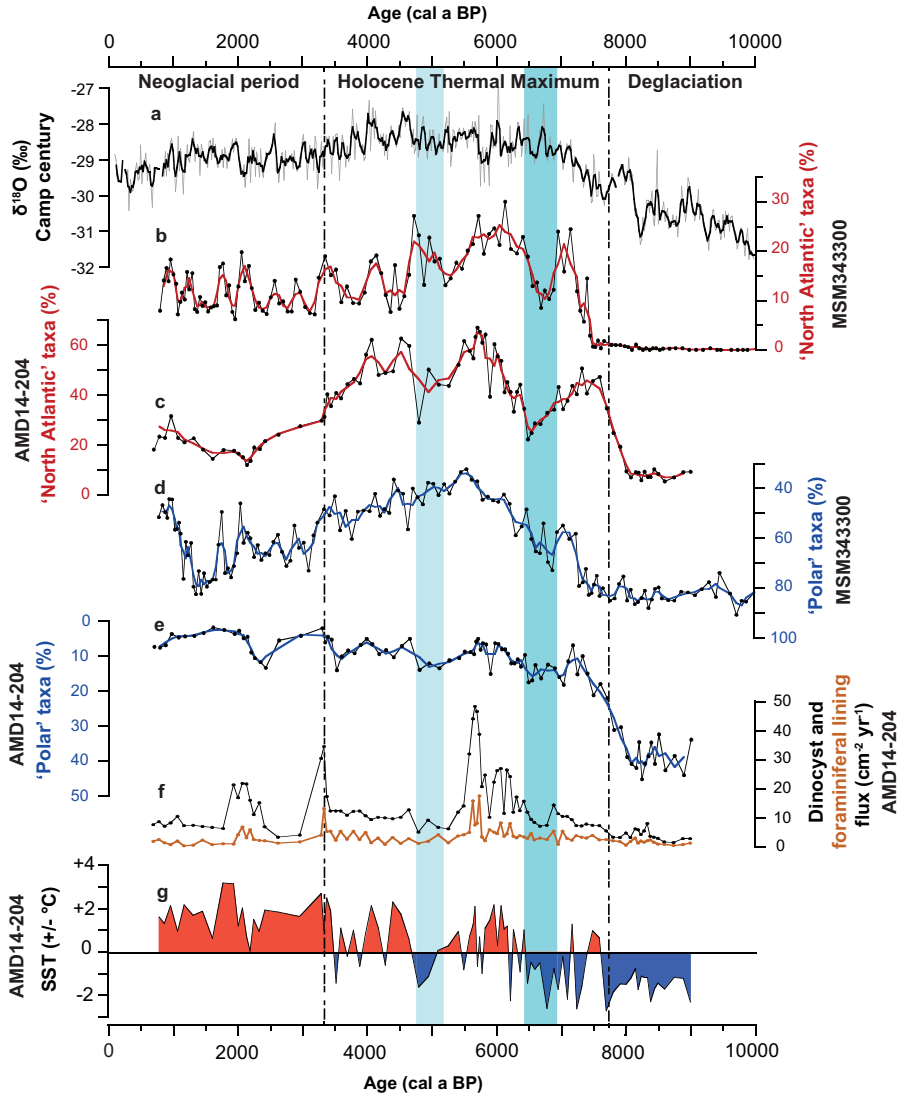


**Figure 7.** Comparison of the palynological records from core AMD14-204 (this study) with (a) the $\delta^{18}O$ of Camp Century (Vinther *et al.*, 2009), (b–c): 'North Atlantic' taxa (*O. centrocarpum, S. elongatus, S. ramosus)* relative abundance of (a) core MSM343300, Disko Bugt (Ouellet-Bernier *et al.*, 2014) and (b) core 204, (d–e): 'Polar' taxa (*I. minutum, E. karaense, Polykrikos* var. Arctic*)* relative abundance (note reversed scale) of (d) core MSM343300 and (e) core 204, (f) dinocysts and foraminiferal linings influxes ($cm^{-2}$ $yr^{-1}$) of core 204 and (g) reconstructed SST anomaly (°C) compared with modern value for core 204. The Holocene Thermal Maximum is delimited by the two dashed lines, and blue shaded areas indicate the two cold pulses (zones 2b and 2d). [Color figure can be viewed at wileyonlinelibrary.com]

and species richness, suggesting milder conditions with warmer SST and a reduced SIC during this period (Figs. 3 and 7). Several regional records (based on dinocysts or foraminifera) have also observed a major shift due to surface and subsurface warming that occurred between 7400 and 7800 cal a BP, which is considered as the transition toward modern postglacial conditions and warmer sea-surface conditions (e.g., Perner *et al.*, 2013; Ouellet-Bernier *et al.*, 2014; Jennings *et al.*, 2014; Gibb *et al.*, 2015). Indeed, the establishment of warmer conditions in Baffin Bay is likely to be a response to the reinforcement of the warm and saline component (IC) of the WGC, linked with the final retreat of both the Laurentide ice sheet and the GIS (Lloyd *et al.*, 2005; Ouellet-Bernier *et al.*, 2014; Gibb *et al.*, 2015). In addition, the dominance of the phototrophic species *O. centrocarpum* and *S. elongatus* is often associated with the North Atlantic Drift, suggesting surface water temperatures >0°C throughout the year (Rochon *et al.*, 1999; Mudie *et al.*, 2006; Zonneveld *et al.*, 2013).

In the Kane Basin, this transition toward interglacial conditions is also marked by the increase of accompanying autotrophic species *O. centrocarpum* and *S. elongatus* from 7880 to 7200 cal a BP, although the assemblage is still dominated by heterotrophic taxa (Fig. 5). This suggests warmer sea-surface conditions, which nonetheless remained relatively cold with an extended SIC, as expected considering the presence of the strong cold Arctic current flowing southward in the basin (Münchow *et al.*, 2006). This is coherent with Levac *et al.* (2001), who suggest sea-surface temperatures up to 3°C higher than at present as early as 7800 $^{14}C$ a BP (~8000 cal a BP) in Smith Sound (Fig. 8). As *O. centrocarpum* and *S. elongatus* are considered as Atlantic water indicators, these results could reflect the entry of warmer Atlantic water into the basin (via the IC) associated with the enhanced strength of the WGC during this period (Perner *et al.*, 2013), the insolation maximum (Lecavalier *et al.*, 2017) and isostatic readjustment after the retreat of grounded ice (England *et al.*, 2006).

## *Middle Holocene – Holocene Thermal Maximum*

Dinocyst assemblages of core 204 indicate that warm postglacial conditions were established in northeastern Baffin Bay after 7750 cal a BP, although two periods (6880–6450 and 5100–4750 cal a BP) are marked by the decrease of *O. centrocarpum* abundance (warm water taxa) and an increase of the abundance of *E. karaense* and *I. minutum* (cold taxa; Fig. 3). These two periods are associated with relatively lower reconstructed SST and productivity values and a higher SIC duration (Fig. 4). These results suggest a temporary return to colder sea-surface conditions during these periods, possibly caused by meltwater pulses from the GIS, also evidenced by moderate peak abundance of *Halodinium* spp. at the top of both subzones. Overall, we associate the period from 7750 to 3350 cal a BP to the Holocene Thermal Maximum (HTM), with optimal conditions observed between 6400 and 5500 cal a BP (Fig. 7). The high dinocyst influx, as well as the relatively high reconstructed SST and

productivity values, supports this interpretation (Figs. 4 and 7), which is also consistent with previous regional work (e.g., Ouellet-Bernier *et al.*, 2014; Jennings *et al.*, 2014). Furthermore, a higher influence of the IC (stronger, saltier and warmer WGC) was recorded between 6200 and 3500 a BP by Perner *et al.* (2013).

As mentioned above, our data from the Kane Basin suggest warmer conditions between 7880 and 7200 cal a BP, with the highest relative abundance of "North Atlantic" indicators. This period is also characterized by maximum influxes of foraminiferal linings (high benthic productivity) and very low dinocyst influxes (Fig. 8). Regional studies (Bradley, 1990; Levac *et al.*, 2001; Knudsen *et al.*, 2008; Jennings *et al.*, 2011; Lecavalier *et al.*, 2017) have recorded an early HTM in this area compared with lower latitude sites (e.g., Disko Bugt or the Labrador Sea). Likewise, Ledu *et al.* (2010) observed an increase of the phototrophic taxa relative abundance, linked with the HTM between 8500 and 5500 cal a BP. Nevertheless, the low dinocyst influxes and high benthic productivity suggest that dinoflagellates may not be solely responsible for the primary productivity in the Nares Strait area, and that diatoms may be involved (Cormier *et al.*, 2016). Thus, our results could reflect relatively open water conditions without ice arch formation during this period, favourable for the development of phototrophic dinocyst species and diatoms.

## *Late Holocene changes in sea-surface conditions*

Regionally, the Late Holocene is characterized by a cooling trend which corresponds to the neoglacial period associated with glacier growth and subsurface cooling along the west Greenland coast (e.g., Briner *et al.*, 2016; Perner *et al.*, 2013; Schweinsberg *et al.*, 2017). This neoglacial cooling period has been recorded over the last ca. 4000 cal a BP in regional reconstructions (e.g., Knudsen *et al.*, 2008; Seidenkrantz *et al.*, 2008; Krawczyk *et al.*, 2010; Andresen *et al.*, 2010). The fluctuations observed in the reconstructed sea-surface conditions at both our sites over the last ca. 3500 cal a BP reflect this cooling to a certain extent after ~2000 cal a BP.

However, after 3350 cal a BP, core 204 is marked by a major change in the dinocyst assemblages with a dominance shift from *O. centrocarpum* to cysts of *P. dalei* (Fig. 3), suggesting changes in surface water conditions during this period, which were not observed in other regional dinocyst records (e.g., Ouellet-Bernier *et al.*, 2014; Gibb *et al.*, 2015). In the Arctic,

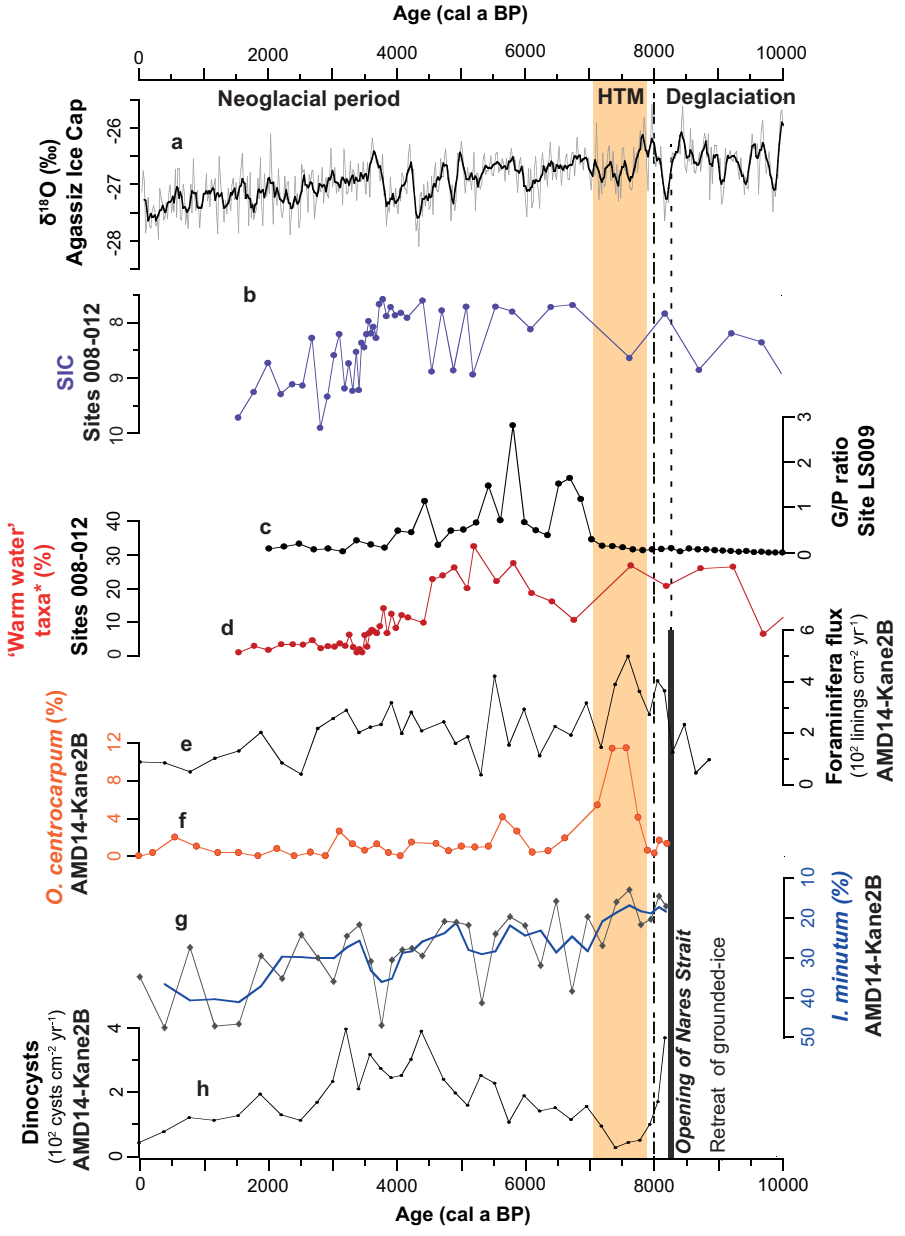


**Figure 8.** Comparison of the palynological records from core AMD14-Kane2B (this study) with (a) the $\delta^{18}O$ temperature reconstructions from the Agassiz Ice Cap (Vinther *et al.*, 2009), (b) SIC duration (months/year) from sites 008 and 012 (Levac *et al.*, 2001), (c) Gonyaulacal/Peridinoid (G/P) ratio from site LS009 (Ledu *et al.*, 2008), (d) 'warm water' taxa (**O. centrocarpum*, *S. elongatus*) relative abundance from sites 008 and 012, (e) foraminiferal lining influxes $cm^{-2}$ $yr^{-1}$, (f) *O. centrocarpum* relative abundance, (g) *I. minutum* relative abundance, (h) dinocyst influxes in cyst $cm^{-2}$ $yr^{-1}$. Data from sites 008, 012 and LS009 (core 2004-804-009) were downloaded from the GEOTOP dinocyst database (de Vernal *et al.*, 2013a). [Color figure can be viewed at wileyonlinelibrary.com]

cysts of *P. dalei* are associated with relatively warm, stratified and highly productive waters, and generally require SST higher than 4°C (Rochon *et al.*, 1999; Matthiessen *et al.*, 2005; Ribeiro *et al.*, 2012). Moreover, a high abundance of cysts of *P. dalei* is recorded in locations with a large seasonal temperature gradient (Rochon *et al.*, 1999). Thus, the dominance of this species, which is found in abundance near Iceland (Zonneveld *et al.*, 2013) could reflect a higher seasonal gradient during this period, possibly from an increased contribution of the Atlantic component (IC) to the WGC. Indeed, warmer SST (increase by ~1.5°C) after ~3.1 cal ka BP was also observed by Gibb *et al.* (2015) and was attributed to enhanced strength of the IC.

Reconstructions from the Kane Basin reflect the abundance of the dominant taxa: *Brigantedinium* spp. for the productivity and SST, and *I. minutum* + *E. karaense* for the SIC duration. We interpret the maximum dinocyst influxes and dominance of *Brigantedinium* spp. between 5200 and 2100 cal a BP to reflect an increased primary productivity linked to the availability of pelagic prey, mostly diatoms (Jacobson and Anderson, 1986; Matthiessen *et al.*, 2005; Cormier *et al.*, 2016), but not necessarily warmer conditions. Besides, we associate the increasing trend of *I. minutum* after 5200 cal a BP with a progressive cooling, possibly linked to the neoglaciation. This cooling trend intensified over the last 2100 cal a BP (increase of *I. minutum, E. karaense* and *Polykrikos* var. Arctic*)* with decreasing dinocyst influxes (Figs. 5 and 8). Indeed, the relative abundance of *I. minutum* increases linearly with the duration of seasonal SIC in Arctic regions (Zonneveld *et al.*, 2013). This is coherent with the work of Levac *et al.* (2001) that observed a general deterioration of sea-surface conditions over the last ~3200 cal a BP in Smith Sound (increased SIC; Fig. 8). Finally, Ledu *et al.* (2008) also recorded a cooling trend in Lancaster Sound starting after 5500 cal a BP. Thus, we suggest that the increase of *I. minutum* and *E. karaense* observed at the top of the core (last 2100 cal a BP) could reflect this regional cooling trend of the Late Holocene.

## Conclusions

Paleoclimatic reconstructions based on dinocyst assemblages from two sediment cores (AMD14-204 and AMD14-Kane2B) using the MAT provided insight into the evolution of sea-surface conditions during the Holocene. In the northeastern Baffin Bay (core 204), the dinocyst assemblages revealed important changes throughout the Holocene, with harsh conditions prior to 7750 cal a BP, associated with an extended SIC and high meltwater inputs from the retreating GIS. A shift to warmer conditions occurred around 7750 cal a BP as a response to the final retreat of the GIS and a strengthened North Atlantic component (IC) of the WGC. From 7750 to 3350 cal a BP, the dominance of phototrophic taxa and highest species richness marks the mid-Holocene thermal optimum associated with warmer SST, higher productivity and reduced SIC, culminating between 6450 and 5100 cal a BP. Finally, after 3350 cal a BP, the progressive establishment of modern dinocyst assemblages is observed, associated with higher seasonality.

In Kane Basin (core Kane2B), our results revealed the dominance of heterotrophic taxa throughout the core. Results suggest relatively cold sea-surface conditions, with abundant SIC during most of the Holocene in this area. Nonetheless, variations of the dinocyst assemblages reveal some changes in the sea-surface conditions following the opening of the Nares Strait (and the strengthened southward flow of cold Arctic water through it). The enhanced contribution of Atlantic water recorded between 7880 and 7200 cal a BP, marked by the occurrence of autotrophic taxa, suggests different oceanographic conditions than the present, likely caused by the insolation maximum and breakup of the IIS. Maximum primary productivity recorded between 5200 and 2100 cal a BP reflects the availability of prey for heterotrophic dinoflagellates. Finally, an increasing abundance of the Arctic taxa *I. minutum* is associated with a progressive cooling trend, which intensified after 2100 cal a BP.

Overall, this study indicates that sea-surface conditions in northeastern Baffin Bay are more favourable for the growth of autotrophic dinoflagellates than in the Nares Strait. This is explained by the influence of the warm and relatively salty WGC on the eastern side of Baffin Bay compared with the strong southward Arctic flow in the Nares Strait. Finally, this study confirmed the important changes in sea-surface conditions that occurred from the end of the deglaciation until present, both for the northwestern Greenland shelf and the Nares Strait. These variations can be associated with changes in meltwater discharges or the varying strength of oceanic currents (e.g., IC or EGC influence), which are themselves related to the main climatic changes of the Holocene.

*Acknowledgements.* We are grateful to the captain, officers, crew and scientists on board the CCGS Amundsen during the 2014 ArcticNet (Leg 1b) expedition for the recovery of cores 204 and Kane2B. This study was supported by ArcticNet, the Natural Sciences and Engineering Research Council of Canada through Discovery Grants to AR, JCMS and GSO, and the CREATE ArcTrain programme through a PhD scholarship to the first author. We thank J. Matthiessen (Alfred-Wegener Institute) for useful advice on dinocyst identification and Q. Beauvais and M-P. St-Onge (UQAR-ISMER) for technical support in the laboratory. We also thank G. Massé (Takuvik) for collecting the cores, MM. Ouellet-Bernier (UQAM) for sharing the MSM343300 sea-surface reconstructions data, as well as E. Georgiadis and J. Giraudeau (U. Bordeaux) for fruitful discussions. Finally, we thank the two anonymous reviewers for their thorough and critical comments, which helped to improve the manuscript.

## Supplementary material

Additional supporting information:

**Fig. S1.** High-resolution images, CT-Scan, age models and sedimentary units for cores AMD14-204 and AMD14-Kane2B. Radiocarbon dates are from Georgiadis *et al.* (2018) for Kane2B and from Caron *et al.* (2019) for core 204; paleomagnetic stratigraphic markers from Caron *et al.* (2019) and organic matter is from Giraudeau *et al.* (under revision). RDL: Rapidly deposited layer.

**Fig. S2.** Results of the principal component analysis as a function of depth (cm) for cores AMD14-204 and AMD14-Kane2B. PC scores are given at the top of each graph, which represent >95% total variance. Dark grey shade (300–320 cm) in core Kane2B corresponds to the RDL (Rapidly Deposited Layer) which marks the final opening of Nares Strait (Georgiadis *et al.*, 2018).

*Abbreviations.* BIC, Baffin Island Current; EGC, East Greenland Current; GIS, Greenland Ice Sheet; HTM, Holocene Thermal Maximum; IC, Irminger Current; IIS, Innuitian Ice Sheet; MAT, modern analogue technique; RDL, rapidly deposited layer; SIC, sea ice cover; SST, sea-surface temperature; SSS, sea-surface salinity; WGC, West Greenland Current.

## References

Aksu AE, Piper DJW. 1987. Late Quaternary sedimentation in Baffin Bay. *Canadian Journal of Earth Science* **24**: 1833–1846.

Allan E, de Vernal A, Knudsen MF, *et al.* 2018. Late Holocene Sea Surface Instabilities in the Disko Bugt Area, West Greenland, in Phase With $\delta^{18}O$ Oscillations at Camp Century. *Paleoceanography and Paleoclimatology* **33**: 227–243.

Andresen CS, McCarthy DJ, Valdemar Dylmer C, *et al.* 2010. Interaction between subsurface ocean waters and calving of the Jakobshavn Isbrae during the late Holocene. *The Holocene* **21**: 211–224.

Barber DG, Hanesiak JM, Chan W, *et al.* 2001. Sea-ice and meteorological conditions in Northern Baffin Bay and the North Water polynya between 1979 and 1996. *Atmosphere-Ocean* **39**(3): 343–359.

Bradley RS. 1990. Holocene paleoclimatology of the Queen Elizabeth Islands, Canadian High Arctic. *Quaternary Science Reviews* **9**(4): 365–384.

Briner JP, McKay NP, Axford Y, *et al.* 2016. Holocene climate change in Arctic Canada and Greenland. *Quaternary Science Reviews* **147**: 340–364.

Caron M, St-Onge G, Montero-Serrano JC. 2019. Holocene chronostratigraphy of northeastern Baffin Bay based on radiocarbon and paleomagnetic data. *Boreas* **48**(1): 147–165.

Cormier MA, Rochon A, de Vernal A, *et al.* 2016. Multi-proxy study of primary production and paleoceanographical conditions in northern Baffin Bay during the last centuries. *Marine Micropaleontology* **127**: 1–10.

Dale B. 1996. Dinoflagellate cyst ecology: modelling and geological applications. In: *Palynology: Principles and Applications*, Jansonius J, McGregory CD (eds). The American Association of Stratigraphic Palynologists Foundation: Salt Lake City: Publishers Press; 1249–1276.

de Vernal A, Bilodeau G, Hillaire-Marcel C, *et al.* 1992. Quantitative assessment of carbonate dissolution in marine sediments from foraminifer linings vs. shell ratios: Davis Strait, northwest North. *Atlantic. Geology* **20**(6): 527–530.

de Vernal A, Henry M, Matthiessen J, *et al.* 2001. Dinoflagellate cyst assemblages as tracers of sea-surface conditions in the Northern North Atlantic, Arctic and sub-Arctic seas: The new "n = 677" data base and its application for quantitative palaeoceanographic reconstruction. *Journal of Quaternary Science* **16**: 681–698.

de Vernal A, Hillaire-Marcel C, Rochon A, *et al.* 2013a. Dinocyst-based reconstructions of sea ice cover concentration during the Holocene in the Arctic Ocean, the northern North Atlantic Ocean and its adjacent seas. *Quaternary Science Review* **79**: 111–121.

de Vernal A, Rochon A, Fréchette B, *et al.* 2013b. Reconstructing past sea ice cover of the Northern Hemisphere from dinocyst assemblages: Status of the approach. *Quaternary Science Reviews* **79**: 122–134.

England JH, Atkinson N, Bednarski J, *et al.* 2006. The Innuitian Ice Sheet: configuration, dynamics and chronology. *Quaternary Science Review* **25**: 689–703.

Fensome RA, Taylor FJR, Norris G, *et al.* 1993. A classification of living and fossil dinoflagellates. *Micropaleontology, Special Publication* **7**.

Georgiadis E, Giraudeau J, Martinez P, *et al.* 2018. Deglacial to postglacial history of Nares Strait, Northwest Greenland: a marine perspective. *Climate of the past* **14**: 1991–2010, https://doi.org/10.5194/cp-2018-78

Gibb OT, Steinhauer S, Frechette B, *et al.* 2015. Diachronous evolution of sea surface conditions in the Labrador Sea and Baffin Bay since the last deglaciation. *The Holocene* **25**: 1882–1897.

Giraudeau J, Georgiadis E, Caron M, et al. under review. A high-resolution elemental record of post-glacial lithic sedimentation in Upernavik Trough, western Greenland: history of ice-sheet dynamics and ocean circulation changes over the last 9 100 years. Global and planetary change.

Guiot J, de Vernal A. 2007. Transfer functions: methods for quantitative paleoceanography based on microfossils. In: *Proxies in Late Cenozoic Paleoceanography. Developments in Marine Geology*, Hillaire-Marcel C, de Vernal A (eds). Elsevier: Amsterdam; 523–563.

Guiot J, de Vernal A. 2011. QSR Correspondence "Is spatial autocorrelation introducing biases in the apparent accuracy of palaeoclimatic reconstructions?" Reply to Telford and Birks. *Quaternary Science Reviews* **21**(30): 3214–3216.

Hammer Ø, Harper DAT, Ryan PD. 2001. PAST: Paleontological Statistics Software Package for Education and Data Analysis. *Palaeontologia Electronica* **4**(1): 9.

Head MJ, Harland R, Matthiessen J. 2001. Cold marine indicators of the late Quaternary: The new dinoflagellate cyst genus *Islandinium* and related morphotypes. *Journal of Quaternary Science* **16**: 621–636.

Jacobson DJ, Anderson DM. 1986. Thecate heterotrophic dinoflagellates: feeding behavior and mechanisms. *Journal of Phycology* **22**: 249–258.

Jakobsson M, Long AJ, Ingólfsson Ó, *et al.* 2010. New insights on Arctic Quaternary climate variability from palaeo-records and numerical modelling. *Quaternary Science Review* **29**: 3349–3358.

Jennings AE, Sheldon C, Cronin T, *et al.* 2011. The Holocene History of Nares Strait: Transition from Glacial Bay to Arctic-Atlantic Throughflow. *Oceanography* **24**: 26–41.

Jennings AE, Walton ME, Ó Cofaigh C, *et al.* 2014. Paleoenvironments during Younger Dryas-Early Holocene retreat of the Greenland Ice Sheet from outer Disko Trough, central west Greenland. *Journal of Quaternary Science* **29**(1): 27–40.

Jennings AE, Andrews JT, Oliver B. 2019. Retreat of the Smith Sound Ice Stream in the Early Holocene. *Boreas* 10.1111/bor.12391

Knudsen KL, Stabell B, Seidenkrantz MS, *et al.* 2008. Deglacial and Holocene conditions in northernmost Baffin Bay: Sediments, foraminifera, diatoms and stable isotopes. *Boreas* **37**: 346–376.

Krawczyk D, Witkowski A, Moros M, *et al.* 2010. Late-Holocene diatom-inferred reconstruction of temperature variations of the West Greenland Current from Disko Bugt, central West Greenland. *The Holocene* **20**: 659–666.

Krawczyk D, Witkowski A, Moros M, *et al.* 2017. Quantitative reconstruction of Holocene sea ice and sea surface temperature off West Greenland from the first regional diatom data set. *Paleoceanography* **32**: 18–40.

Kwok R, Toudal Pedersen L, Gudmandsen P, Pang SS. 2010. Large sea ice outflow into the Nares Strait in 2007. *Geophysical Research Letters* **37**(3): L03502. 10.1029/2009GL041872

Lecavalier BS, Fisher DA, Milne GA, *et al.* 2017. High Arctic Holocene temperature record from the Agassiz ice cap and Greenland ice sheet evolution. *Proceedings of the National Academy of Sciences* 114(23): 5952–5957.

Ledu D, Rochon A, de Vernal A, *et al.* 2008. Palynological evidence of Holocene climate change in the eastern Arctic: A possible shift in the Arctic oscillation at the millennial time scale. *Canadian Journal of Earth Science* **45**: 1363–1375.

Ledu D, Rochon A, de Vernal A, *et al.* 2010. Holocene paleoceanography of the northwest passage, Canadian Arctic Archipelago. *Quaternary Science Reviews* **29**(25-26): 3468–3488.

Levac E, de Vernal A, Blake WJ. 2001. Sea-surface conditions in northernmost Baffin Bay during the Holocene: Palynological evidence. *Journal of Quaternary Science* **16**: 353–363.

Lloyd JM, Park LA, Kuijpers A, *et al.* 2005. Early Holocene palaeoceanography and deglacial chronology of Disko Bugt, west Greenland. *Quaternary Science Reviews* **24**(14-15): 1741–1755.

Londeix L, Zonneveld K, Masure E. 2018. Taxonomy and operational identification of Quaternary species of *Spiniferites* and related genera. *Palynology* **42**(sup1): 45–71.

Lovejoy C, Legendre L, Martineau MJ, *et al.* 2002. Distribution of phytoplankton and other protists in the North. *Water. Deep Sea Research Part II: Topical Studies in Oceanography* **49**(22-23): 5027–5047.

Matthews J. 1969. The assessment of a method for the determination of absolute pollen frequencies. *New Phytologist* **68**(1): 161–166.

Matthiessen J. 1995. Distribution patterns of dinoflagellate cysts and other organic-walled microfossils in recent Norwegian-Greenland Sea sediments. *Marine Micropaleontology* **24**: 307–334.

Matthiessen J, de Vernal A, Head M, *et al.* 2005. Modem organic-walled dinoflagellate cysts in arctic marine environments and their (paleo-) environmental significance. *Paläontologische Zeitschrift* **79**(1): 3–51.

Mertens KN, Verhoeven K, Verleye T, *et al.* 2009. Determining the absolute abundance of dinoflagellate cysts in recent marine sediments: the Lycopodium marker-grain method put to the test. *Review of Palaeobotany and Palynology* **157**(3): 238–252.

Mertens KN, Van Nieuwenhove N, Gurdebeke PR, *et al.* 2018. The dinoflagellate cyst genera *Achomosphaera* Evitt 1963 and *Spiniferites* Mantell 1850 in Pliocene to modern sediments: a summary of round table discussions. *Palynology* **42**(sup1): 10–44.

Mudie PJ. 1992. Circum-Arctic Quaternary and Neogene marine palynofloras: paleoecology and statistical analysis. *Neogene and Quaternary dinoflagellate cysts and acritarchs* **10**: 347–390.

Mudie PJ, Harland R, Matthiessen J, *et al.* 2001. Marine dinoflagellate cysts and high latitude Quaternary paleoenvironmental reconstructions: an introduction. *Journal of Quaternary Science* **16**(7): 595–602.

Mudie PJ, Rochon A, Prins MA, *et al.* 2006. Late Pleistocene-Holocene Marine Geology of Nares Strait Region: Palaeoceanography from Foraminifera and Dinoflagellate Cysts, Sedimentology and Stable Isotopes. *Polarforschung* **74**(1-3): 169–183.

Müller J, Stein R. 2014. High-resolution record of late glacial and deglacial sea ice changes in Fram Strait corroborates ice-ocean interactions during abrupt climate shifts. *Earth and Planetary Science Letter* **403**: 446–455.

Münchow A, Melling H, Falkner KK. 2006. An observational estimate of volume and freshwater flux leaving the Arctic Ocean through Nares Strait. *Journal of Physical Oceanography* **36**(11): 2025–2041.

Ouellet-Bernier MM, de Vernal A, Hillaire-Marcel C, *et al.* 2014. Paleoceanographic changes in the Disko Bugt area, West Greenland, during the Holocene. *The Holocene* **24**: 1573–1583.

Perner K, Moros M, Jennings AE, *et al.* 2013. Holocene palaeoceanographic evolution off West Greenland. *The Holocene* **23**: 374–387.

Radi T, de Vernal A. 2008. Dinocysts as proxy of primary productivity in mid-high latitudes of the Northern Hemisphere. *Marine Micropaleontology* **68**: 84–114.

Radi T, Bonnet S, Cormier MA, *et al.* 2013. Operational taxonomy and (paleo-) autecology of round, brown, spiny dinoflagellate cysts from the Quaternary of high northern latitudes. *Marine Micropaleontology* **98**: 41–57.

Ribeiro S, Moros M, Ellegaard M, *et al.* 2012. Climate variability in West Greenland during the past 1500 years: Evidence from a high-resolution marine palynological record from Disko Bay. *Boreas* **41**: 68–83.

Rochon A, de Vernal A, Turon JL, *et al.* 1999. Distribution of recent dinoflagellate cysts in surface sediments from the North Atlantic Ocean and adjacent seas in relation to sea-surface parameters. *American Association of Stratigraphic Palynologists Contribution Series* **35**: 1–146.

Sadler HE. 1976. Water, heat, and salt transports through Nares Strait, Ellesmere Island. *Journal of the Fisheries Research Board of Canada* **33**: 2286–2295.

Schweinsberg AD, Briner JP, Miller GH, *et al.* 2017. Local glaciation in West Greenland linked to North Atlantic Ocean circulation during the Holocene. *Geology* **45**(3): 195–198.

Seidenkrantz MS, Roncaglia L, Fischel A, *et al.* 2008. Variable North Atlantic climate seesaw patterns documented by a late Holocene marine record from Disko Bugt, West Greenland. *Marine Micropaleontology* **68**: 66–83.

Serreze MC, Stroeve J. 2015. Arctic sea ice trends, variability and implications for seasonal ice forecasting. *Philosophical Transactions of the Royal Society A* **373**(2045): 20140159.

Telford RJ. 2006. Limitations of dinoflagellate cyst transfer functions. *Quaternary Science Reviews* **25**(13-14): 1375–1382.

Telford RJ, Birks HJB. 2005. The secret assumption of transfer functions: problems with spatial autocorrelation in evaluating model performance. *Quaternary Science Reviews* **24**(20-21): 2173–2179.

Telford RJ, Birks HJB. 2011. A novel method for assessing the statistical significance of quantitative reconstructions inferred from biotic assemblages. *Quaternary Science Reviews* **30**(9-10): 1272–1278.

Tang CCL, Ross CK, Yao T, *et al.* 2004. The circulation, water masses and sea-ice of Baffin Bay. *Progress in Oceanography* **63**: 183–228.

Vinther BM, Buchardt SL, Clausen HB, *et al.* 2009. Holocene thinning of the Greenland ice sheet. *Nature* **461**(7262): 385.

Zonneveld KAF, Marret F, Versteegh GJM, *et al.* 2013. Atlas of modern dinoflagellate cyst distribution based on 2405 data points. *Review of Palaeobotany and Palynology* **191**: 1–197.

Zweng MM, Münchow A. 2006. Warming and freshening of Baffin Bay, 1916–2003. *Journal of Geophysical Research: Oceans* **111**(C07016).

 